https://doi.org/10.1590/jatm.v18.1440 ORIGINAL PAPER

Blade Twist and Disc Loading Effects on the Rotor Aerodynamics in the Vortex Ring State Modes

Pavel Viacheslavovich Makeev[1,*]

1. Moscow Aviation Institute – National Research University – Aeronautical Engineering – Moscow – Russia.

*Corresponding author: makeevpv@mai.ru

ABSTRACT

The article is dedicated to parametric studies of the effect of the rotor blade twist θ_{tw} and the rotor disc loading P values on rotor aerodynamics in the vortex ring state (VRS) modes. Sixteen rotor configurations with a loading P in the range of 150 to 600 Pa (in hovering), with a blade twist θ_{tw} in the range of 8° to -16°, have been considered. The original free wake model of a rotor has been used for a numerical study. For each of the 16 rotors, the vertical (axial) descent modes (angle of attack of a rotor $\alpha_R = 90°$) in the range of descent speeds $V_y = 0$ to 26 $m \cdot s^{-1}$ were investigated. For two selected rotors, the steep descent modes ($\alpha_R = 80°$ to 20°) were additionally investigated. The dependences of rotor thrust on the velocity of descent for a fixed blade pitch angle $\theta(V_y)$ were analyzed. The boundaries of the VRS modes area have been plotted. The obtained results have demonstrated the significant influence of the θ_{tw} and P parameters on the rotor aerodynamics and on the VRS area boundaries. The data obtained can be used in preliminary design and in the process of choosing initial parameters of the helicopter main rotor, and are also useful in developing the future concepts of variable-twist rotors.

Keywords: Free wake model; Rotor; Blade twist; Rotor disc loading; Vortex ring state modes.

INTRODUCTION

The geometric layout of a helicopter rotor is of a highly complex design, involving numerous parameters. One of the primary areas of focus in helicopter engineering is optimization of rotor design. While maintaining the same overall blade planform shape and airfoil set, the main rotor may have varying numbers of blades, blade twist angles, and arrangements for the spatial positioning of the blades (e.g., single, co-axial or scissor-type rotors) (Ignatkin *et al.* 2018).

The geometric layout has a significant effect on the performance of the helicopter's main rotor in the hovering mode.

This issue is also of significant practical interest for other modes of flight. In particular, it is important to investigate the impact of the geometric layout of the rotor on its aerodynamic characteristics in vertical and steep descent conditions within the context of vortex ring state (VRS) phenomena.

The aerodynamic characteristics of a rotor in VRS conditions exhibit many features, including an increase in required power, a decrease in thrust, unsteady pulsations of aerodynamic forces and moments, specific shapes of the vortical wake, and flow patterns around the rotor. These features present challenges for helicopter pilots and can make VRS conditions unsafe.

The analysis of the aerodynamic characteristics of the rotor allows for the determination of the VRS boundaries in terms of inflow velocity coordinates "V_x-V_y." These boundaries are included in the helicopter operating manual as a special area where flight is not permitted.

Received: Sep. 16, 2025 | **Accepted:** Apr. 14, 2026
Peer Review History: Single Blind Peer Review.
Section editor: SungKi Jung

Despite the fact that studies of the VRS modes have been carried out using various methods since the late 1940s, it is not yet possible to state that this phenomenon has been comprehensively and exhaustively analyzed. Flight research into VRS conditions is limited both in terms of its capabilities and due to its inherent dangers (Akimov 1988; Jimenez *et al*. 2001; Petrosian 2004; Yeates 1958). Experimental (modeling) research poses significant technical challenges and material costs (Azuma and Obata 1968; Babenko *et al*. 2022; Betzina 2001; Castles and Gray 1951; Chae *et al*. 2022; Drees and Hendal 1951; Empey and Ormiston 1974; Pickles *et al*. 2023; Stack *et al*. 2005; Veismann *et al*. 2023; Washizu *et al*. 1966; Xin and Gao 1996; Yaggy and Mort 1963).

The results of various investigations of rotor aerodynamics in VRS modes are typically presented in a relatively non-dimensional form. To achieve this, the inflow and induced velocities are divided by the value of induced velocity in the hover mode, and thrust and torque coefficients are divided by their values in the hovering mode. Despite this, an analysis of various findings reveals a significant reliance on the testing conditions and parameters of the rotor under study (Johnson 2005), rendering an accurate comparison of the different results with one another inapplicable.

Therefore, the task of investigating the influence of the geometric layout of an aircraft on its aerodynamic characteristics and on the boundaries of VRS modes is of significant importance.

With the development of helicopter rotor theory, as well as the growth of computing capabilities, the possibility of numerical modeling of various problems of rotor aerodynamics has become very important. However, the VRS modes, due to their features, also represent one of the most serious challenges for numerical modeling. Due to their assumptions, many calculation methods do not allow the analysis of the entire set of phenomena associated with the VRS modes (Peters and Chen 1982; Shaidakov 1960; Tyabrisova and Ivchin 1997; Vozhdaev 1970; Wolkovitch 1972). The practical application of the most modern approaches based on the solution of the Navier-Stokes equations by finite volume methods is difficult due to their extreme resource intensity (Kinzel *et al*. 2019; Mohd and Baracos 2017; Stalewski and Surmacz 2020).

In previous experimental and computational studies, there has been a lack of a comprehensive and extended parametric study of the impact of the geometric layout of the rotor and the rotor disc loading values on aerodynamic performance in the VRS modes. The results obtained are often conflicting. This is supported by the findings of several studies (Brown *et al*. 2002; Castles and Gray 1951; Petrosian 2004; Tyabrisova and Ivchin 1997).

Obviously, the issue of the influence of the geometric layout on the aerodynamic performance of the rotor in VRS modes requires extensive parametric investigations. This approach would allow the analysis of the net effect of specific parameters, while eliminating their mutual interaction and extraneous influences.

Taking into account the progress in the development of computer technology, the most relevant tool for such research today is modern applied computational models that combine sufficient speed and accuracy in modeling the real physics of the rotor in the VRS modes. These are primarily modern free wake models (Anikin 2002; Belotserkovskii *et al*. 1992; Brown *et al*. 2002; Celi and Ribera 2007; Krimskiy and Sheglova 2014; Leishman *et al*. 2002; Şenipek *et al*. 2023).

A free wake model of a rotor developed at the Moscow Aviation Institute meets the above requirements (Ignatkin *et al*. 2009). Based on this model, a method for calculating the aerodynamic characteristics of the rotor in the VRS modes has been developed, which has been widely used in the study of VRS modes of helicopter main and tail rotors (Makeev *et al*. 2021a; b; 2022).

This paper presents the results of a parametric study of the influence of the most significant rotor parameters: the rotor blade twist and the rotor disc loading, on the rotor aerodynamics and on the VRS modes area boundaries.

Free wake model

The free wake model of a rotor developed at the MAI Helicopter Design Department refers to grid-free methods for calculating fluid flow. This method is also known as the vortex-lattice method. It is based on the Lagrangian approach, which considers the motion of individual particles in a continuum. These particles are discrete vortex segments that simulate the rotor blades and their free wake. Outside the vortex system, the flow is assumed to be potential.

A more detailed description of the free wake model and its main principles can be found in the works of Ignatkin *et al*. (2009) and Makeev *et al*. (2021a). A brief overview of the free wake model's fundamentals is presented below.

The free wake model scheme is illustrated in Fig. 1. This model utilizes the lifting line and blade element theories. Each rotor blade is composed of several rectangular elements, which are modeled as attached vortex segments of length Δr located at a quarter of the chord length c (Fig. 1a). A control point is positioned in the center of each vortex segment (Fig. 1a). The local induced velocities and aerodynamic forces are determined at these control points. The aerodynamic forces and moments acting on each element (Fig. 1b) are then summed to calculate the overall forces and moments on the rotor hub.

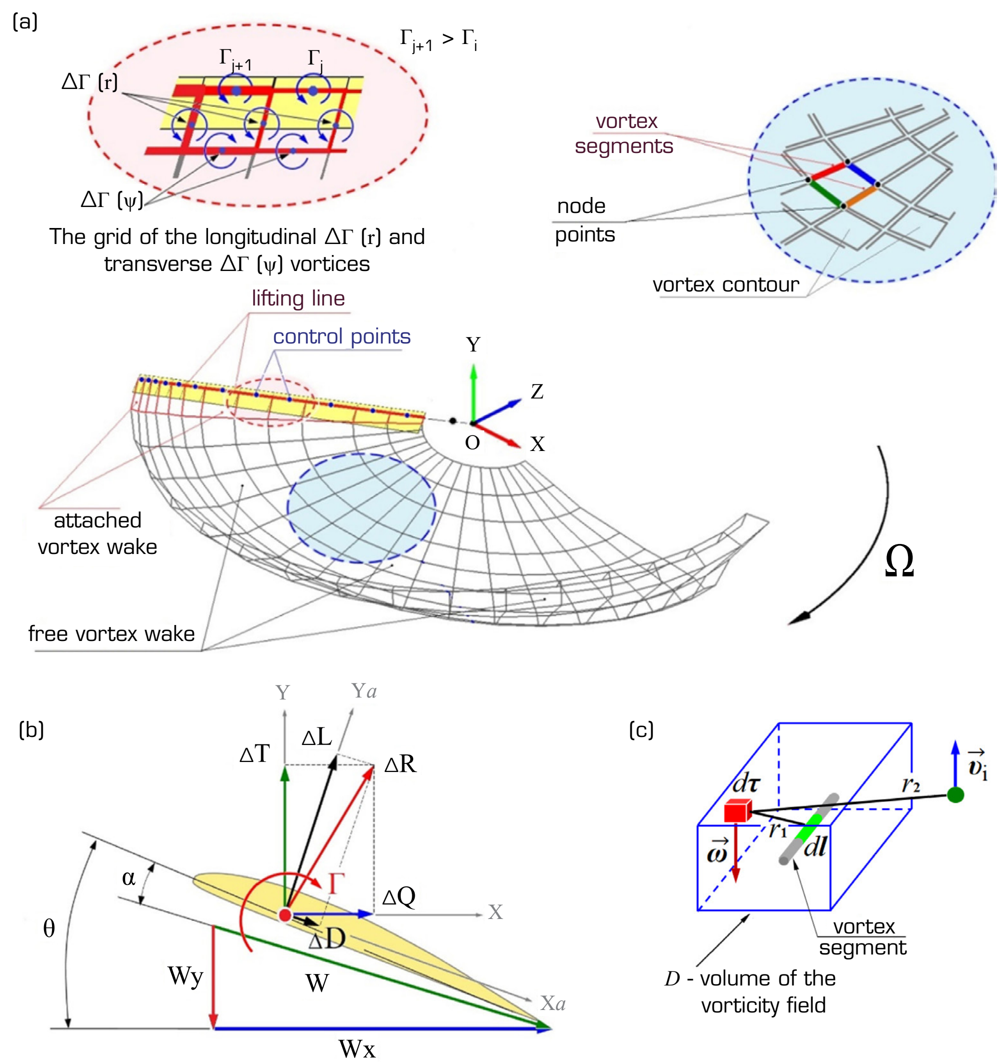

Source: Elaborated by the authors.

Figure 1. Free wake model of a rotor. (a) The formation of the free vortex wake behind the rotor blade; b) Velocities and forces on the blade element; c) Calculation of the induced velocity υ_i from a diffusing vortex segment dl.

During the rotation of the blade, for each blade element, a closed vortex contour descends at a time interval Δt corresponding to the azimuthal angle Δψ. The circulation Γ of this vortex contour is equal to the current circulation of the attached vortex of the blade element (Fig. 1a).

The circulation Γ of the attached vortex may vary within the blade radius r and over the azimuthal angle ψ. Over the rotor revolutions, a system of closed quadrangular vortex contours develops around the rotor blades, forming a free vortex wake. The vortex wake behind the blade can be represented as a grid of discrete longitudinal ΔΓ(r) and transverse vortices ΔΓ (ψ), which connect at node points (Fig. 1a).

The free vortex wake elements (vortex segments) move in a velocity field consisting of the rotational velocities of the blades ωr, the flapping motion velocities υ_β of the blades (if present), the incoming flow V, and the induced velocities υ_i.

The circulation Γ of the vortex segment attached to the blade element (Fig. 1a) is determined by the Kutta-Zhukovsky theorem using an iterative method (Makeev *et al.* 2021a).

To calculate the induced velocity from a diffusing vortex segment (Fig. 1c), an original model (Ignatkin *et al.* 2009; Makeev *et al.* 2021a) is used, which makes it possible to obtain a stable solution in VRS modes characterized by high complexity and nonlinearity of the vortex wake structures behind the rotor.

Object of study and assumptions

The article is dedicated to parametric studies of the effect of the blade twist θ_{tw} and the disc loading P values on the helicopter main rotor aerodynamics in the VRS modes. This issue requires parametric computational studies.

Sixteen different rotors have been considered in the parametric studies. The rotors were numbered for convenience from 1 to 16, and their parameters are shown in Table 1.

Table 1. Parameters of the rotors under study.

No.	r0, m	R, m	ωR, m·s⁻¹	σ	nb	θtw, °	P, Pa
1	2	10	220	0.04	2	8	150
2	2	10	220	0.04	2	0	150
3	2	10	220	0.04	2	-8	150
4	2	10	220	0.04	2	-16	150
5	2	10	220	0.08	4	8	300
6	2	10	220	0.08	4	0	300
7	2	10	220	0.08	4	-8	300
8	2	10	220	0.08	4	-16	300
9	2	10	220	0.12	4	8	450
10	2	10	220	0.12	4	0	450
11	2	10	220	0.12	4	-8	450
12	2	10	220	0.12	4	-16	450
13	2	10	220	0.16	6	8	600
14	2	10	220	0.16	6	0	600
15	2	10	220	0.16	6	-8	600
16	2	10	220	0.16	6	-16	600

Source: Elaborated by the authors.

All the considered rotors had the following fixed parameters: rotational speed of blade tips ωR = 220 m/s, blade radius R = 10 m, blade root radius r_0 = 2 m, blade shape in plan: rectangular, blade airfoils NACA 230-12. The variable rotor parameters were: blade twist θ_{tw} = 8º, 0º, -8º, and -16º (Fig. 2), rotor solidity σ = 0.04, 0.08, 0.12, and 0.16, rotor disc loading (in hovering) P = 150, 300, 450, and 600 Pa (c_T = 0.005, 0.01, 0.015, and 0.02). The number of rotor blades changed from n_b = 2 to 6 with increasing rotor disc loading P (Fig. 3). The considered values of θ_{tw}, P, and n_b cover the entire range used on the main rotors of modern helicopters, except for the positive twist of θ_{tw} = 8°. Positive blade twist is used on the main rotors of gyroplanes and was considered for comparison.

One of the main and most common features of VRS modes, as observed in both experimental and computational studies, is a decrease in rotor thrust (thrust drop) at various descent speeds V_y compared to the hovering mode (at a fixed rotor blade pitch angle $\theta[V_y]$ = const). Based on the magnitude of this thrust drop, the intensity the negative impact of VRS modes on the rotor aerodynamic performance can be estimated. The size of the thrust drop area determines the boundaries of the VRS modes.

The influence of θ_{tw} and P parameters on rotor aerodynamics was estimated based on the analysis of the rotor thrust coefficient dependences $c_T = f(V_y)$ at fixed rotor blade pitch angles $\theta(V_y)$ = const. Axial flow modes (α_R = 90°) were considered in the range of descent rates V_y = 0-26 m·s⁻¹with a step ΔV_y = 1-2 m·s⁻¹ The rotor blades were considered absolutely rigid and without flapping motion. Each rotor blade was divided into 12 calculated elements. The calculated time step was Δψ = 12°. The estimated number of rotor revolutions for each of the considered regimes was n = 120.

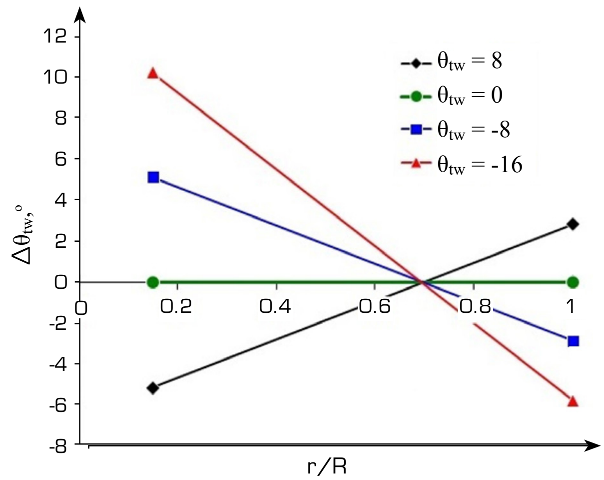

Source: Elaborated by the authors.

Figure 2. Distributions of the twist along the rotor blade radius.

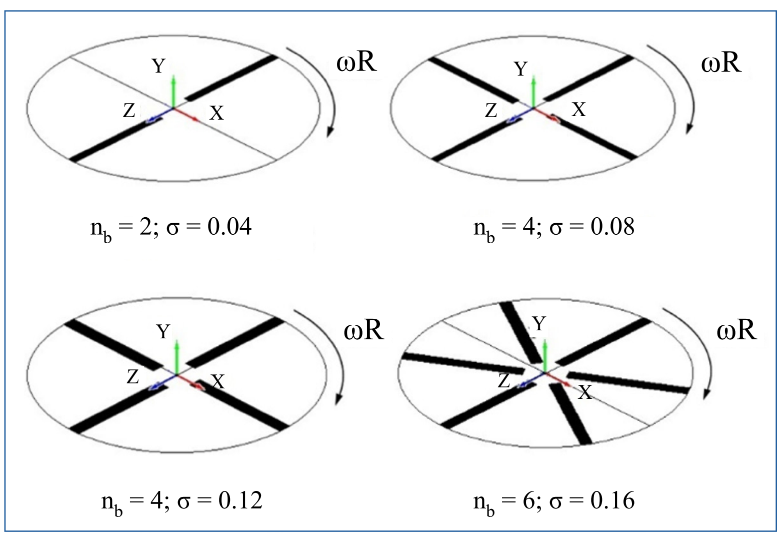

Source: Elaborated by the authors.

Figure 3. Calculated rotors visualizations.

Validation

Widely known experimental data from the works of Azuma and Obata (1968) and Washizu *et al*. (1966) were used to validate the free wake model in the VRS modes. The authors used two different types of experimental rigs to study the VRS modes. In the first case, the rotor was mounted on a movable trolley and moved along rails in a hydraulic channel about 200 meters long (Washizu *et al*. 1966). The second experimental rig was a conventional wind tunnel with a diameter of the working section of 3 meters, where the rotor was installed (Azuma and Obata 1968). In both experiments, the rotor had the following parameters: number of blades $n_b = 3$; blade tip rotational speed $\omega R = 57.5$ m·s^{-1} rotor radius $R = 0.55$ m; blade shape was rectangular in plan, $r_0/R= 0.15$; $c = 0.033$ m; blade airfoil NACA-0012; blade twist $\theta_{tw} = -8.3°$.

Various characteristics were obtained in the works (Azuma and Obata 1968; Washizu *et al*. 1966), including the dependences of the rotor thrust on the incoming flow velocity V at fixed blade pitch angles θ. The observed decrease in rotor thrust compared to the hover mode is one of the main features of the VRS modes. These data were used to validate the computational model. The results of comparing the experimental data obtained by Azuma and Obata (1968) and Washizu *et al*. (1966) with the results of numerical simulation are presented below.

Figure 4 shows the dependence of the rotor thrust coefficient $c_T = f(V_y)$ in axial flow modes ($\alpha_R = 90°$) for various values of the total pitch $\theta(V_y) = const$. Here, the flow velocity V_y is represented in relative non-dimensional form: $V_y/\omega R$. The calculation results in Fig. 4 are presented in the form of time-averaged thrust coefficients c_{Tav}. The experimental (Washizu *et al.* 1966) dependences of c_T in Fig. 4 are presented in the form of solid regions that take into account the variation of c_T values due to thrust pulsations in the VRS modes. There is satisfactory agreement between the calculated and experimental results.

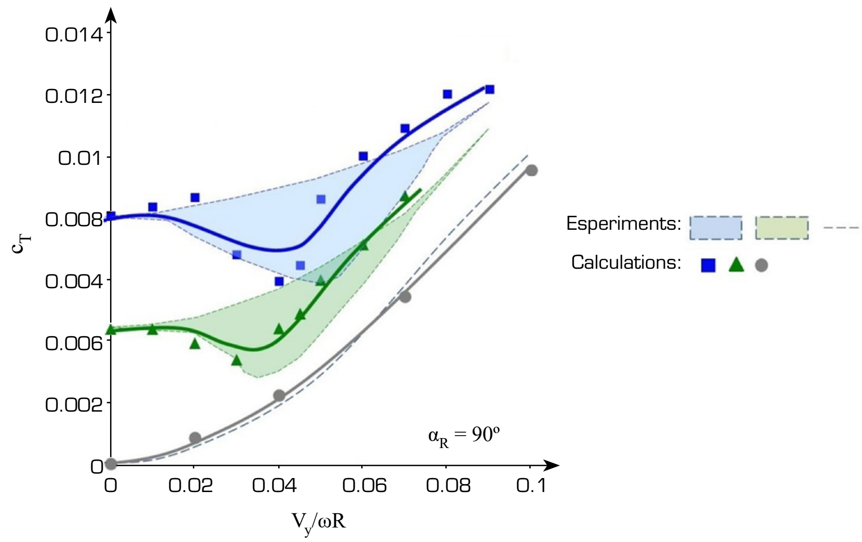

Source: Elaborated by the authors.

Figure 4. Dependences of $c_T = f(V_y/\omega R)$ (Washizu et al. 1966).

Figure 5 shows the experimental dependences of $c_{Tav}/c_{Th} = f(V_y)$ from (Azuma and Obata 1968) and the calculated results. The thrust coefficient is presented in the relative form c_{Tav}/c_{Th}, which means it is related to the hovering thrust coefficient c_{T0}. The flow velocity V_y is related to the average induced velocity in the hovering mode, υ_{ih}, defined as $\upsilon_{ih} = 0.5 \cdot \omega R \cdot c_{Th}{}^{1/2}$. Figure 5 also demonstrates a good agreement between the calculated results and experimental data.

Thus, the free wake model reflects the features of the aerodynamic characteristics of the rotor in the VRS modes observed in experiments.

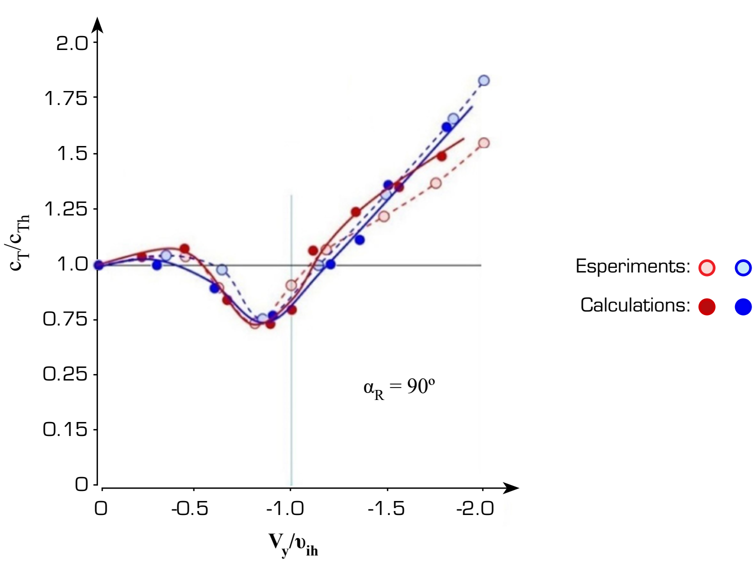

Source: Elaborated by the authors.

Figure 5. Dependences of $c_{Tav}/c_{Th} = f(V_y/\upsilon_{ih})$ (Azuma and Obata 1968).

RESULTS AND DISCUSSION

As mentioned above, the study considers four values of rotor disc loading P = 150, 300, 450, and 600 Pa, and four blade twist angle values: θ_{tw} = 8, 0, -8, and -16°. This gives 16 different combinations of P and θ_{tw}.

The obtained calculation results are grouped in a way to evaluate the effect of P at θ = const and the effect of θ_{tw} at P = const. This approach allows considering both parameters P and θ_{tw} independently and analyzing the "clean" effects of their influence on the rotor aerodynamics in the VRS modes.

Figure 6 shows diagrams of the dependence of the rotor time-averaged relative thrust coefficient $c_{Tav}/c_{Th} = f(V_y/\upsilon_{ih})$. The dependences are constructed for the blade twist values θ_{tw} = 8, 0, -8, and -16° and P = const.

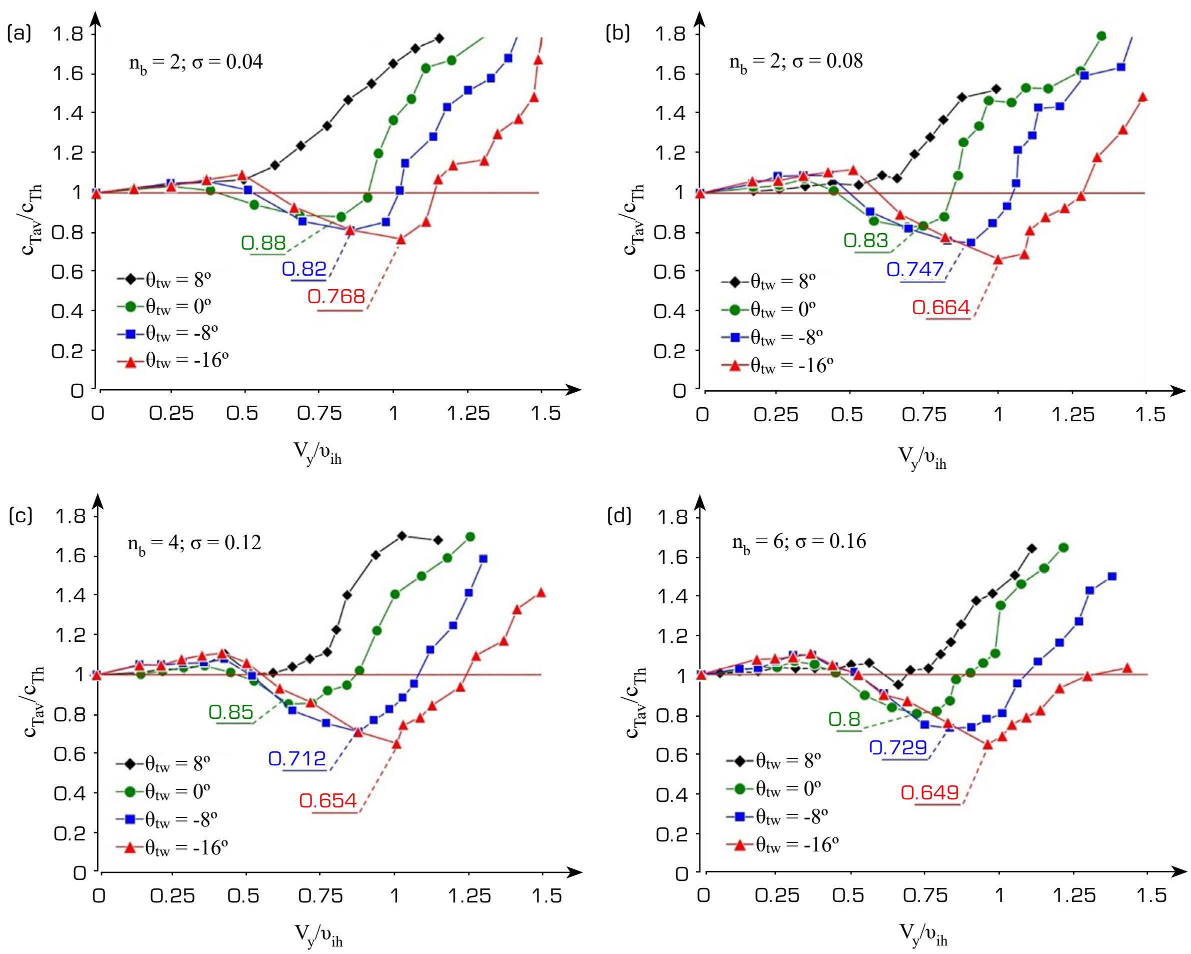

Source: Elaborated by the authors.

Figure 6. Dependences of $c_{Tav}/c_{Th} = f(V_y/\upsilon_{ih})$. (a) Rotors no. 1-4 (P = 150 Pa); (b) Rotors no. 5-8 (P = 300 Pa); (c) Rotors no. 9-12 (P = 450 Pa); (d) Rotors no. 13-16 (P = 600 Pa).

The results show that the region of the VRS modes, which is determined by the criterion $c_{Tav}/c_{Th} < 1$, shifts to the right with an increase in the negative twist of the blades and expands significantly with the velocity V_y/υ_{ih}. For example, for P = 150 Pa (Fig. 6a), the lower boundary of the VRS modes for θ_{tw} = 0° corresponds to the velocity V_y/υ_{ih} = -0.9, and for θ_{tw} = -16°, the velocity V_y/υ_{ih} = -1.1. With increasing rotor disc loading P, this difference becomes greater. At P = 300 Pa (Fig. 6b) and P = 450 Pa (Fig. 6c), the lower boundary for θ_{tw} = -16° corresponds to the velocity V_y/υ_{ih} = -1.2, and at P = 600 Pa (Fig. 6d) and θ_{tw} = -16°, the lower boundary is observed at the velocity V_y/υ_{ih} = -1.32.

In addition to the direct increase in the size of the VRS region with respect to the velocity V_y/υ_{ih}, with an increase in negative twist, the drop in the c_{Tav}/c_{Th} coefficient also increases. For example, at P = 150 Pa and $\theta_{tw} = 0°$ (Fig. 6a), the coefficient c_{Tav}/c_{Th} decreases to 0.88 (by 12%), and at $\theta_{tw} = -16°$, to 0.77 (by 23%). At P = 600 Pa, this drop is already 0.8 (20%) and 0.65 (35%) for $\theta_{tw} = 0°$ and -16°, respectively (Fig. 6d). That is, as the rotor disc loading P increases, the thrust drop in the VRS modes also increases.

From Fig. 6, it can also be noted that in the case of a positive "autogyro" rotor blade twist $\theta_{tw} = 8°$ at the considered values of P = 150, 300, 450, and 600 Pa, a drop in the relative thrust $c_{Tav}/c_{Th} < 1$ is practically not observed over the entire descent speed range.

Diagrams in Figs. 7 and 8 are constructed for a comprehensive analysis of the blade twist θ_{tw} and disc loading P effects on the rotor aerodynamics in the VRS modes. They show the influence of θ_{tw} and P parameters on the maximum thrust drop values.

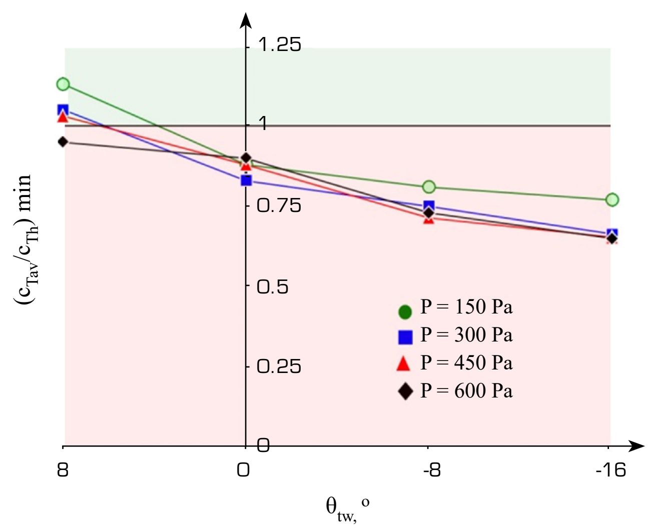

Source: Elaborated by the authors.

Figure 7. The effects of the blade twist θ_{tw} on the thrust drop values.

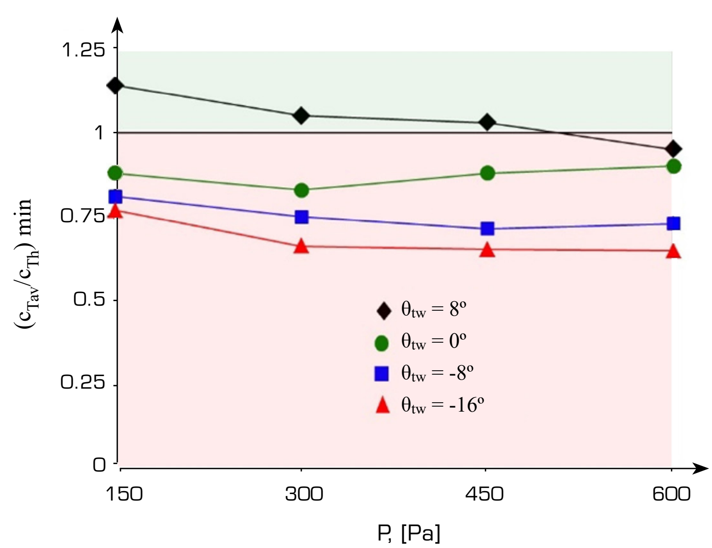

Source: Elaborated by the authors.

Figure 8. The effect of the rotor disc loading P on the thrust drop values.

Figure 7 shows a diagram $(c_{Tav}/c_{Th})_{min} = f(\theta_{tw})$ illustrating the effect of blade twist θ_{tw} on the magnitude of the maximum thrust drop in the VRS modes. Four dependences correspond to the loads P = 150, 300, 450, and 600 Pa. It can be seen that the blade twist has a significant effect on the thrust drop of the rotor. With a positive twist of θ_{tw} = 8°, there is no drop in thrust, and with a negative twist of θ_{tw} = -16°, thrust drops by 35% compared to the hover mode.

Figure 8 shows the diagram $(c_{Tav}/c_{Th})_{min} = f(P)$ for various fixed values of the blade twist θ_{tw} = 8°, 0°, -8°, and -16°. It can be seen here that the effect of the loading P on the drop in rotor thrust is weak.

Thus, the use of negative twist and an increase of its values up to θ_{tw} = -8 and -16° lead to an increase in the magnitude of the thrust drop in the VRS modes. The use of a positive blade twist θ_{tw} = 8° leads, on the contrary, to the actual absence of the thrust drop in the VRS modes.

These effects can be explained by the analysis of the working conditions of the rotor airfoils along the blade radius for various rotor flow modes and blade twist values. As an example, the use of various blade twists for rotors having a rotor disc loading in the hovering mode P = 450 Pa (see rotors no. 9-12 in Table 1) is considered.

Firstly, the blade twist effect on the rotor efficiency in the hover mode is considered. Figure 9 shows the dependences of the figure of merit (FoM) = $f(c_T/\sigma)$. It can be seen that negative θ_{tw} values lead to a significant increase in FoM values. When the blade twist is changed from 0° to -16°, the FoM increases by almost 18%. On the contrary, using a positive blade twist θ_{tw} = 8° leads to a decrease in FoM by 9%.

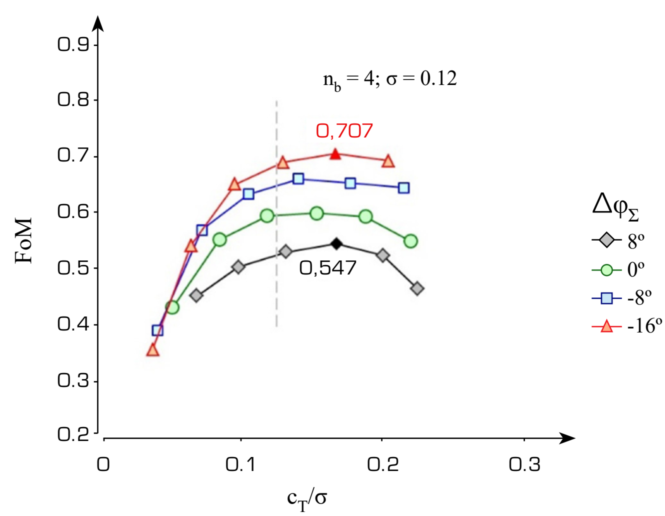

Source: Elaborated by the authors.

Figure 9. FoM diagrams for rotors no. 9-12.

The effect of blade twist on the VRS modes is then considered. The maximum thrust drop at twist θ_{tw} = 8, 0, -8, and -16° (rotors no. 9-12 in Table 1) was observed at descent speeds V_y = 8, 8, 10, and 11 $m{\cdot}s^{-1}$, respectively. The dependences $c_T = f(n)$ for these modes, as well as the dependences for the hover mode (c_{Th} = 0.015= const), are shown in Fig. 10. Significant unsteady thrust pulsations over time are observed, which is a distinctive feature of the VRS modes. It can be seen that the time-averaged (taking into account pulsations) thrust values c_{Tav}, presented as lines, decrease significantly when using negative blade twist. At θ_{tw} = -16°, the c_{Tav} drops by almost 35%, while for a positive twist θ_{tw} = 8°, there is no drop in the average thrust over time.

Figure 11 shows the calculated shapes of the vortex wake for rotor no. 11 (θ_{tw} = -8 and P = 450 Pa). The shapes of the vortex wake for different rotor revolution numbers n are shown. For convenience, Fig. 11 shows only the vortices coming off the ends of the blades. The toroidal structure of the vortex wake of the rotor, characteristic of the VRS modes, is observed. It is also seen that the shape and position of the vortex wake change significantly over time, which causes the thrust pulsations shown in Fig. 10. Figure 12 demonstrates a picture of the flow around the rotor using streamlines. There is a circulating flow around the rotor, which is also a characteristic of the VRS modes.

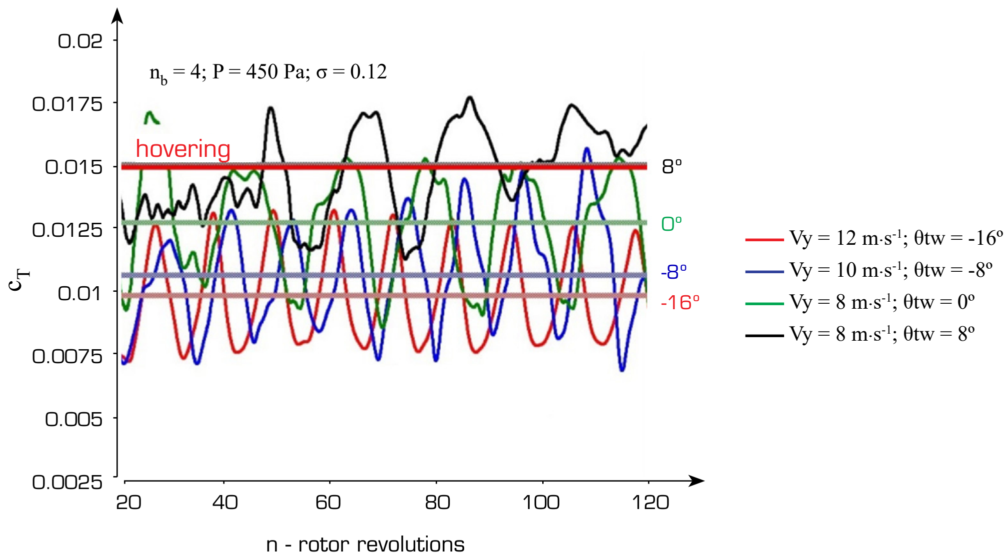

Source: Elaborated by the authors.

Figure 10. Dependences of $c_T = f(n)$ at the VRS modes (rotors no. 9-12).

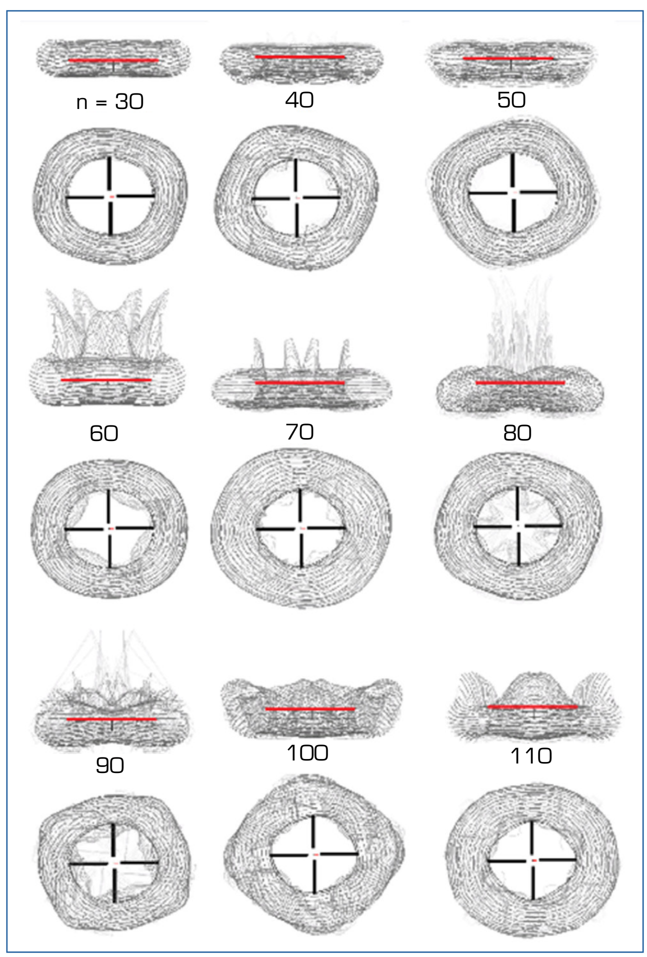

Source: Elaborated by the authors.

Figure 11. Vortex wake shapes, rotor no. 11 ($V_y = 10$ m·s^{-1}).

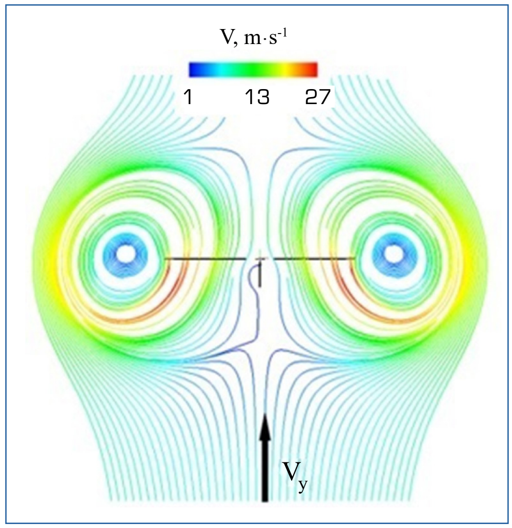

Source: Elaborated by the authors.

Figure 12. Rotor flow visualization, rotor no. 11 (V_y = 10 m·s^{-1}).

The operating conditions of rotor blades in hover and VRS modes are considered, compared, and analyzed.

Figures 13 and 14 show the dependence of the distribution of the airfoil's angle of attack along the non-dimensional blade radius α = f(r/R).

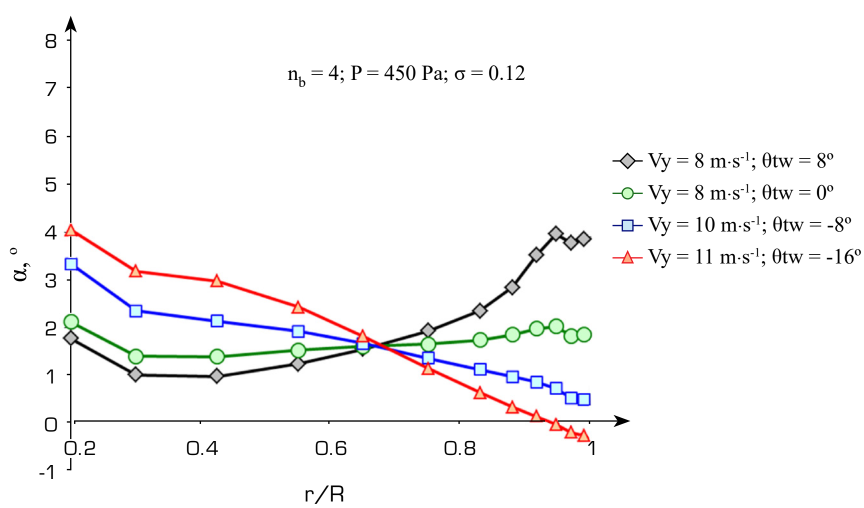

Source: Elaborated by the authors.

Figure 13. Dependences of α_{av} = f(r/R) at the VRS modes.

Figure 13 shows the dependences of α = f(r/R) for the VRS modes (Fig. 10). The angles of attack vary over time due to thrust pulsations in the VRS modes, so Fig. 13 shows their time-averaged values α_{av}. Figure 14 shows the dependences α = f(r/R) for hovering modes. It can be seen that blade twist significantly affects the distribution of angles of attack along the blade radius. The dependences α = f(r/R) for θ_{tw} = -8° and -16°, which provide maximum hovering efficiency (maximum FoM values in Fig. 9), give a more uniform distribution of angles of attack along the blade. Twists of θ_{tw} = 8° and 0° in hovering (Fig. 14), on the contrary, lead to small angles of attack at the root of the blade and large ones at the blade tip. This causes an increase in power consumption and a decrease in efficiency. In the VRS modes, large negative twists are accompanied by a sharp decrease in the angles of attack at the tip of the blade, which leads to a significant drop in rotor thrust.

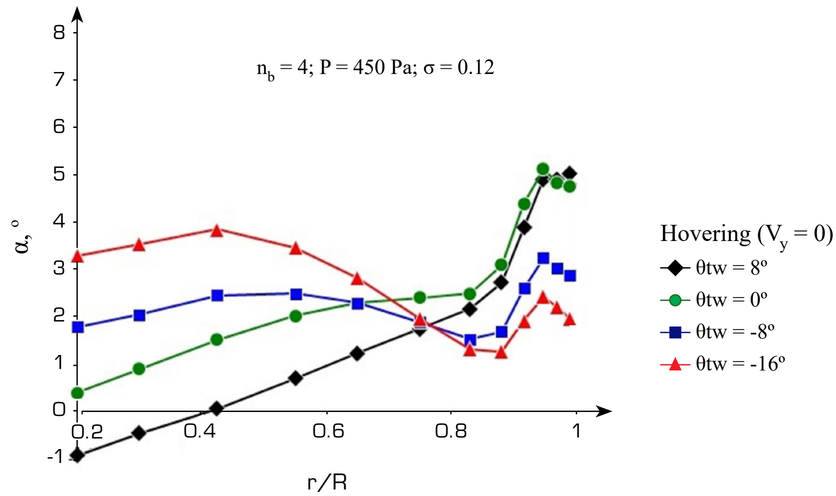

Source: Elaborated by the authors.

Figure 14. Dependences of α = f(r/R) in the hovering modes.

A more favorable distribution for the time-averaged angle of attack α_{av} = f(r/R) in the VRS mode is observed for a positive blade twist θ_{tw} = 8°. There is no sharp decrease in the angle of attack at the tip of the blade (Fig. 13). As shown in Fig. 6b, there are also no drops in time-averaged rotor thrust despite the VRS modes.

Therefore, with positive blade twist, the VRS modes proceed without a significant drop in the time-averaged rotor thrust and, accordingly, without an increase in the required power, that is, without a significant part of the negative effects.

The use of positive blade twist values on helicopter rotors is impractical due to the low hovering efficiency (Fig. 9). However, in the case of the development of the blades with variable "active" blade twist, performing a steep descent with such a blade twist law will obviously be more favorable.

Figure 15 shows the diagram summarizing the dependences of time-averaged rotor thrust coefficients c_{Tav}/c_{Th} = f(V_y/υ_{ih}) for all 16 rotor configurations considered (Table 1). The effect of the rotor disc loading P is shown as an area corresponding to the considered disc loading range P = 150-600 Pa. Each area has its own color corresponding to one of the blade twist values θ_{tw} = 8°,

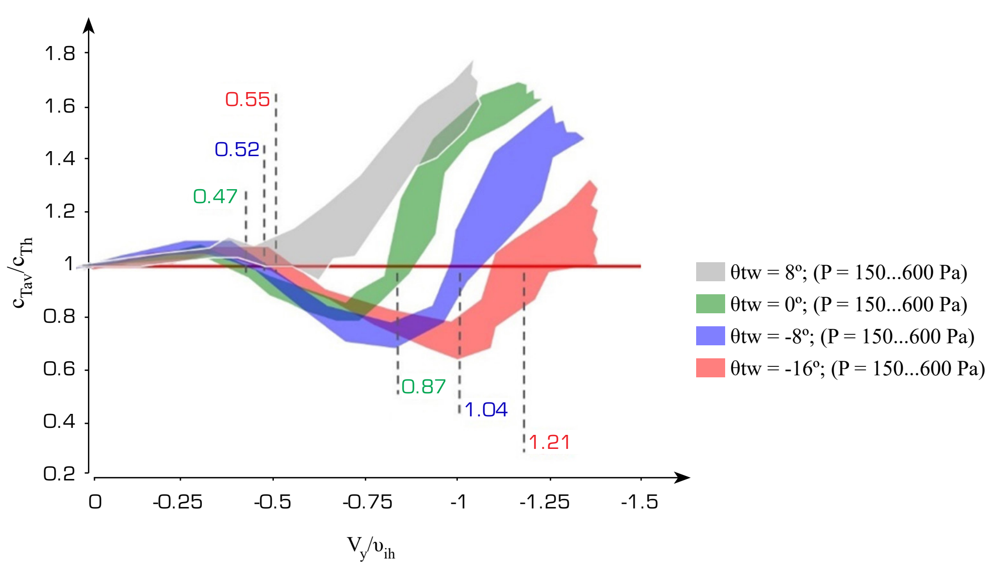

Source: Elaborated by the authors.

Figure 15. Diagrams of c_{Tav}/c_{Th} = f(V_y/υ_{ih}) at various θ_{tw} and P values.

0°, -8°, or -16°. It is clearly seen that the boundaries of the VRS modes at different disc loadings P are stratified and shift with increasing P to the right along the velocity V_y/υ_{ih} by 8-14%. It also follows from Fig. 15 that the effect of the blade twist on the VRS boundaries (especially on the lower boundary) is large and reaches 40% with an increase in the negative twist from θ_{tw} = 0° to -16°.

Figure 16 shows the diagram summarizing the dependences of the thrust pulsation amplitudes $(\Delta c_T/2)/c_{Tav} = f(V_y/\upsilon_{ih})$ for all 16 rotor configurations considered. This diagram complements the diagram in the Fig. 10 and has the same principle of representation with colorized solid areas for each particular blade twist value in the considered disc loading range. Figure 16 demonstrates the influence of blade twist and disc loading on the rotor thrust pulsation amplitudes. It can be seen that an increase in loading and twist leads to a significant increase in the amplitude of thrust pulsations from 10-12% to 80-90%. At the same time, the positive twist of the blade θ_{tw} = 8° is almost the same as the negative twist θ_{tw} = -8° in terms of thrust pulsations

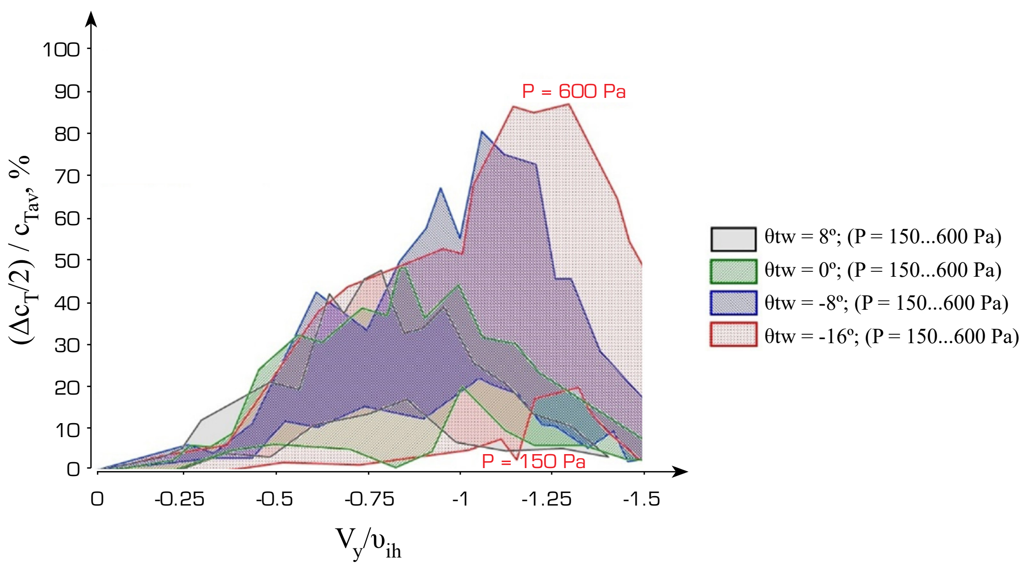

Source: Elaborated by the authors.

Figure 16. Diagrams of $(\Delta c_T/2)/c_{Tav} = f(V_y/\upsilon_{ih})$ at various θ_{tw} and P values.

The obtained results prove that it is important to take into account both the parameters, the blade twist θ_{tw} and rotor disc loading P, which significantly and comprehensively affect the rotor aerodynamic characteristics and the VRS modes boundaries. The magnitude of the loading must have noticeable effects on the constructed VRS boundaries, even in the special non-dimensional velocity coordinates V_y/υ_{ih}.

The results shown in Figs. 15 and 16 relate to axial flow modes (vertical descent), when the angle of attack of a rotor α_R = 90°. Thus, they are not complete and exhaustive, since the full boundaries of the VRS region are plotted in coordinates V_x-V_y, including steep descent modes with forward flight velocity V_x.

Modeling steep descent modes with different speeds V_y and angles α_R for all 16 rotors considered is an extremely difficult task. To avoid this, a limited calculation of the VRS boundaries was performed for only two rotor configurations. For this purpose, the rotors with the greatest difference in aerodynamic characteristics were selected (according to Fig. 15). The positive blade twist θ_{tw} = 8° was not considered, since it is not used on helicopter rotors. Therefore, rotors no. 2 (P = 150 Pa; θ_{tw} = 0°) and no. 16 (P = 600 Pa; θ_{tw} = -16°) were used for comparison. In fact, they correspond to the parameters of the main rotors of light and heavy helicopters.

For the mentioned rotors, the steep descent modes for α_R = 80-20° with a step of 10° were additionally investigated. The grid of calculated modes required for this is shown in Fig. 17 and amounts to about 150 modes for each rotor. To determine the VRS boundary in the steep descent modes, as well as for vertical (axial) descent modes, the criterion of reducing the relative thrust of the $c_{Tav}/c_{Th} < 1$ was used.

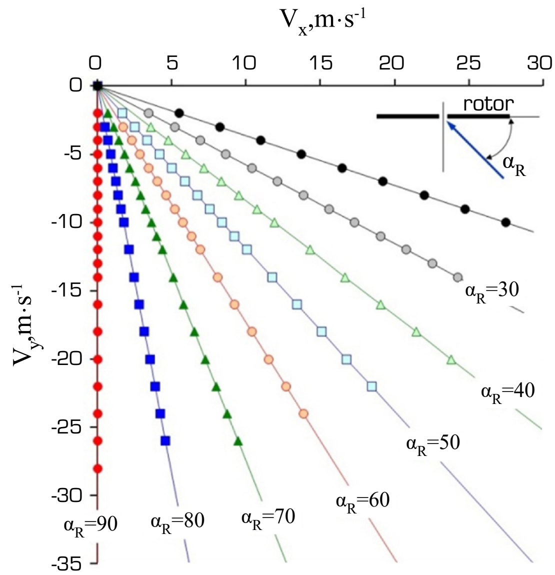

Source: Elaborated by the authors.

Figure 17. Grid of calculation regimes for study step descent modes of a rotor.

As a result of analyzing the obtained aerodynamic characteristics dependences, the boundaries of the VRS modes area were constructed in relative velocity coordinates $V_x/\omega R$-$V_y/\omega R$. The resulting diagram is shown in Fig. 18. It can be seen that the dimensions of the VRS modes area for both rotors differ significantly. Rotor no. 16 (P = 600 Pa; θ_{tw} = -16°) has a range of the VRS modes area almost twice as large in both width and height.

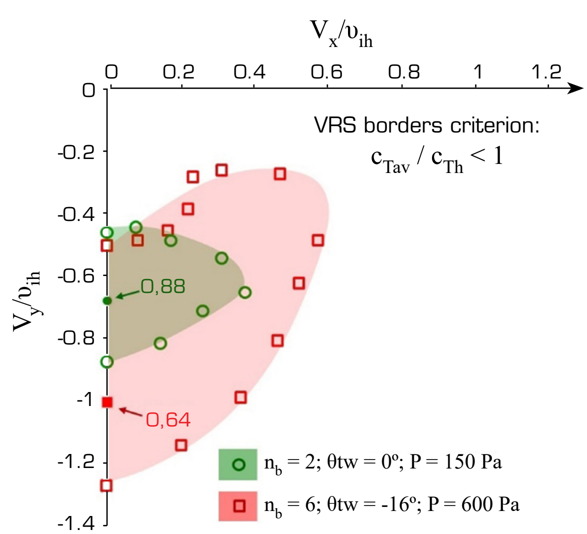

Source: Elaborated by the authors.

Figure 18. Calculated VRS boundaries in non-dimensional velocity form.

The obtained results explain the significant differences in the boundaries of the VRS modes area observed when comparing data from various experimental studies in non-dimensional form. These differences in the VRS boundaries can be explained not only by the specifics of a particular experiment (differences in the methods used, experimental rigs, possible errors, etc.), but also by differences in the parameters of the rotors themselves.

Thus, the obtained results demonstrate the impossibility of using the boundaries of the VRS modes area in non-dimensional form as is common for any rotors. They indicate the need to study the VRS boundaries taking into account the individual parameters of the rotor.

CONCLUSION

Numerical parametric studies of the helicopter main rotor aerodynamics with different blade twist and rotor disc loading values in the VRS modes area have been performed. Vertical and steep descent modes at a fixed blade pitch angle of the rotor have been considered.

The dependences of rotor thrust coefficients and rotor thrust pulsation amplitudes on the vertical descent speed have been obtained and analyzed.

It was shown that the blade twist angles and the rotor disc loading parameters have a significant complex effect on the aerodynamic characteristics of a rotor and on the VRS modes area boundaries represented in non-dimensional form and non-dimensional velocity coordinates. In particular, with the simultaneous growth of blade twist from 0 to -16° and disc loading from 150 to 600 Pa, the VRS modes zone increased by 65% in the non-dimensional coordinate V_y/V_{ih}; the magnitude of the thrust drop increased threefold from 12 to 36% of the thrust in hovering; the amplitudes of the rotor thrust pulsations increased almost fourfold and reached 70-90% of the average thrust.

It was confirmed that it is impossible to obtain common boundaries of the VRS modes area in non-dimensional form, and that it is necessary to determine them taking into account the individual characteristics of the rotors.

It has been found that the use of positive blade twist makes it possible to avoid a strong decrease in rotor thrust and, consequently, an increase in the required power in the VRS modes. This conclusion can be used to improve flight safety in VRS modes in rotors designs with variable "active" blade twist.

CONFLICTS OF INTEREST

Nothing to declare.

DATA AVAILABILITY STATEMENT

The data will be available upon request.

FUNDING

Not applicable.

DECLARATION OF USE OF ARTIFICIAL INTELLIGENCE TOOLS

The author declares that no artificial intelligence tools were used in the preparation, writing, data analysis, or review of this manuscript.

ACKNOWLEDGMENTS

Not applicable.

REFERENCES

Akimov AI (1988) Aerodynamics and performance of helicopters. Moscow: Mashinostroenie.

Anikin VA (2002) Helicopter main rotor aerodynamic performance in descent conditions. Paper presented 2002 58th Annual Forum of the American Helicopter Society. AHS; Montreal, Canada.

Azuma A, Obata A (1968) Induced flow variation of the helicopter rotor operating in the vortex ring state. J Aircr 5(4): 381-386. https://doi.org/10.2514/3.43954

Babenko G, Efimov V, Kiselev M, Shkurin M (2022) Results of the study of the influence of external cargo parameters on the helicopter controllability. Aerospace 9(229). https://doi.org/10.3390/aerospace9050229

Belotserkovskii SM, Loktev BE, Nisht MI (1992) Computer-assisted research of the aerodynamic and elastic properties of helicopter rotors. Moscow: Mashinostroenie.

Betzina MD (2001) Tiltrotor descent aerodynamics: a small-scale experimental investigation of vortex ring state. Paper presented 2001 57th Annual Forum of the American Helicopter Society. AHS; Washington, D.C., USA.

Brown RE, Leishman JG, Newman SJ, Perry FJ (2002) Blade twist effects on rotor behaviour in the vortex ring state. Paper presented 2002 28th European Rotorcraft Forum. ERF; Bristol, UK.

Castles J, Gray RB (1951) Empirical relation between induced velocity, trust, and rate of descent of a helicopter rotor as determined by wind-tunnel tests on four model rotors. Washington (DC): NACA. Report No.: TN-2474.

Celi R, Ribera M (2007) Time marching simulation modeling in axial descending through the vortex ring state. Paper presented 2007 63rd Annual Forum of the American Helicopter Society. AHS; Virginia Beach, USA.

Chae S, Lee S, Kim J (2022) Effects of rotor-rotor interaction on the wake characteristics of twin rotors in axial descent. J Fluid Mech 952. https://doi.org/10.1017/jfm.2022.913

Drees J, Hendal WP (1951) Airflow patterns in the neighbourhood of helicopter rotors: a description of some smoke tests carried out in a wind-tunnel at Amsterdam. Aircr Eng Aerosp Technol 23:107-11. https://doi.org/10.1108/eb032021

Empey RW, Ormiston RA (1974) Tail-rotor thrust on a 5.5-foot helicopter model in ground effect. Paper presented 1974 30th Annual Forum of the American Helicopter Society. AHS; Washington, D.C., USA.

Ignatkin YM, Makeev PV, Grevtsov BS, Shomov AI (2009) A non-linear blade vortex propeller theory and its applications to estimate aerodynamic characteristics for helicopter main rotor and anti-torque rotor. Vestnik MAI 16(5):24-31.

Ignatkin YM, Makeev PV, Shomov AI (2018) Calculated research of influence of helicopter main rotors' geometry on the efficiency in hover mode based on the nonlinear vortex model. Civil Aviation High Technologies 2018;21(6):43-53. https://doi.org/10.26467/2079-0619-2018-21-6-43-53

Jimenez J, Desopper A, Taghizad A, Binet L (2001) Induced velocity model in steep descent and vortex-ring state prediction. Paper presented 2001 27th European Rotorcraft Forum. ERF; Moscow, Russia.

Johnson W (2005) Model for vortex ring state influence on rotorcraft flight dynamics. Washington (DC): NASA. Report No.: NASA/TP-2005-213477.

Kinzel MP, Cornelius JK, Schmitz S, Palacios JL, Langelaan JW, Adams D, Lorenz R (2019) An investigation of the behavior of a coaxial rotor in descent and ground effect. Paper presented 2019 AIAA Scitech 2019 Forum. AIAA; San Diego, USA. https://doi.org/10.2514/6.2019-1098

Krimskiy VS, Shcheglova VM (2014) The investigation of rotors inflow and main rotors induced at hover and at steep descent. Civil Aviation High Technologies (200):86-90.

Leishman JG, Bhagwat MJ, Ananthan S (2002) Free-vortex wake predictions of the vortex ring state for single rotor and multi-rotor configurations. Paper presented 2002 58th Annual Forum of the American Helicopter Society. AHS; Montreal, Canada.

Makeev PV, Ignatkin YM, Shomov AI (2021a) Numerical investigation of full scale coaxial main rotor aerodynamics in hover and vertical descent. Chin J Aeronaut 34(5):666-683. https://doi.org/10.1016/j.cja.2020.12.011

Makeev PV, Ignatkin YM, Shomov AI (2021b) Numerical study of the main rotor steep descent modes in the vortex ring state area. J Phys Conf Ser 1925. https://doi.org/10.1088/1742-6596/1925/1/012004

Makeev PV, Ignatkin YM, Shomov AI (2022) Ivchin, V.A. Comparative study of 3-bladed and scissors tail rotors aerodynamics in axial flow. Int Rev Aerosp Eng 15(2). https://doi.org/10.15866/irease.v15i2.21284

Mohd RN, Barakos G (2017) Performance and wake analysis of rotors in axial flight using computational fluid dynamics. J Aerosp Technol Manag 9:193-202. https://doi.org/10.5028/jatm.v9i2.623

Peters DA, Chen SY (1982) Momentum theory, dynamic inflow, and the vortex ring state. J Am Helicopter Soc 27(3). https://doi.org/10.4050/JAHS.27.18

Petrosian EA (2004) Aerodynamics of coaxial helicopter. Moscow: Poligon-Press.

Pickles D, Zagaglia D, Busse A, Green R (2023) Vortex ring state of a shrouded rotor: an experimental survey. Exp Fluids 64. https://doi.org/10.1007/s00348-023-03609-8

Şenipek M, Okcu ID, Tekinalp O, Leblebicioğlu K (2023) System identification of E-VTOL rotor in vortex ring state by viscous vortex particle method. Paper presented 2023 49th European Rotorcraft Forum. ERF; Buckeburg, Germany.

Shaidakov VI (1960) Theoretical research into helicopter rotor operation in vertical descent states. Izv Vuz Av Tekhnika 3(1).

Stack J, Caradonna FX, Savas Ö (2005) Flow visualizations and extended thrust time histories of rotor vortex wakes in descent. J Am Helicopter Soc 50(3). https://doi.org/10.4050/1.3092864

Stalewski W, Surmacz K. (2020) Investigations of the vortex ring state on a helicopter main rotor using the URANS solver. Aircr Eng Aerosp Technol 92(9). https://doi.org/10.1108/AEAT-12-2019-0264

Tyabrisova NU, Ivchin VA (1997) Computational modeling of induced velocities at positive-value rotor angles of attack, and calculations of ring vortex boundaries. Trudy MVZ im. M.L. Milya.

Veismann M, Dougherty C, Gharib M (2023) Effects of rotor separation on the axial descent performance of dual-rotor configurations. Flow 3. https://doi.org/10.1017/flo.2022.31

Vozhdaev ES (1970) rotor theory for the vortex ring states. Trudy TSAGI 1184.

Washizu K, Azuma A, Koo J, Oka T (1966). Experiments on a model helicopter rotor operating in the vortex ring state. J Aircr 3:225-30. https://doi.org/10.2514/3.43729

Wolkovitch J (1972) Analytical prediction of vortex-ring state boundaries for helicopters in steep descents. J Am Helicopter Soc 17(3). https://doi.org/10.4050/JAHS.17.13

Xin H, Gao Z (1996) A prediction of the helicopter vortex-ring state boundary. J Exp Fluid Mech 1:14-19.

Yaggy PF, Mort KW (1963) Wind-tunnel tests of two VTOL propellers in descent. Washington (DC): NASA. Report No.: NASA TN D-1766.

Yeates JE (1958) Flight measurements of the vibration experienced by a tandem helicopter in transition, vortex-ring state, landing approach, and yawed flight. Washington (DC): NACA. Report No.: NACA TN 4409.